Key Points:
- A satellite water balance and AMHG are used to tune PCR-GLOBWB over the Nile
- The method is simple, easily implemented, and needs no in situ data
- More testing is needed to verify these methods in different environments, but this initial demonstration is encouraging

Correspondence to:
C. J. Gleason,
cjgleason@umass.edu

A Hybrid of Optical Remote Sensing and Hydrological Modeling Improves Water Balance Estimation

Colin J. Gleason[1], **Yoshihide Wada[2,3]**, and **Jida Wang[4]**

[1]Department of Civil and Environmental Engineering, University of Massachusetts, Amherst, MA, USA, [2]International Institute for Applied Systems Analysis, Laxenburg, Austria, [3]Faculty of Geosciences, Department of Physical Geography, Utrecht University, Utrecht, the Netherlands, [4]Department of Geography, Kansas State University, Manhattan, KS, USA

Abstract Declining gauging infrastructure and fractious water politics have decreased available information about river flows globally. Remote sensing and water balance modeling are frequently cited as potential solutions, but these techniques largely rely on these same in-decline gauge data to make accurate discharge estimates. A different approach is therefore needed, and we here combine remotely sensed discharge estimates made via at-many-stations hydraulic geometry (AMHG) and the PCR-GLOBWB hydrological model to estimate discharge over the Lower Nile. Specifically, we first estimate initial discharges from 87 Landsat images and AMHG (1984–2015), and then use these flow estimates to tune the model, all without using gauge data. The resulting tuned modeled hydrograph shows a large improvement in flow magnitude: validation of the tuned monthly hydrograph against a historical gauge (1978–1984) yields an RMSE of 439 m^3/s (40.8%). By contrast, the original simulation had an order-of-magnitude flow error. This improvement is substantial but not perfect: tuned flows have a 1–2 month wet season lag and a negative base flow bias. Accounting for this 2 month lag yields a hydrograph RMSE of 270 m^3/s (25.7%). Thus, our results coupling physical models and remote sensing is a promising first step and proof of concept toward future modeling of ungauged flows, especially as developments in cloud computing for remote sensing make our method easily applicable to any basin. Finally, we purposefully do not offer prescriptive solutions for Nile management, and rather hope that the methods demonstrated herein can prove useful to river stakeholders in managing their own water.

1. Introduction

Freshwater is arguably the most important resource required by civilizations, and it drives industry, agriculture, and ecosystem function the world over. Rivers in particular occupy pride of place in providing freshwater resources (despite almost complete dependence on groundwater in certain areas), and humans have settled in river valleys since the dawn of civilization in the Fertile Crescent. Approximately two fifths of total global rainfall eventually winds its way through rivers before reaching the sea (Oki & Kanae, 2006; Vörösmarty et al., 2010), yet despite this vast importance we have a surprisingly poor grasp on how much water is flowing through our rivers globally. The prime reason for this difficulty is a decline in monitoring infrastructure (i.e., gauging stations). These river gauges have been a mainstay of providing flow information to the global community, but are in sharp decline due to expense of maintenance (Hannah et al., 2011; Vörösmarty et al., 2010) or are withheld from the public knowledge for political reasons (Gleason & Hamdan, 2015) (Figure 1). This decline of gauge information has broader impacts beyond the loss of publically available measurements of flow: gauges are also a prime driver of hydrologic modeling, where they are used as calibration and tuning data to assure that models represent particular watersheds as accurately as possible. In addition, calibrated models provide detailed flow information in spatially distributed reaches, essentially extending point gauge measurements in space. We often have historical records from a less-politically sensitive and better-funded era, and yet many of these records are more than a decade old and reflect watersheds that are changed from those we know today. This loss of data means that the crucially needed future assessments of water resources that result from well-calibrated and validated models used in conjunction with future climate scenarios suffer from greater uncertainty.
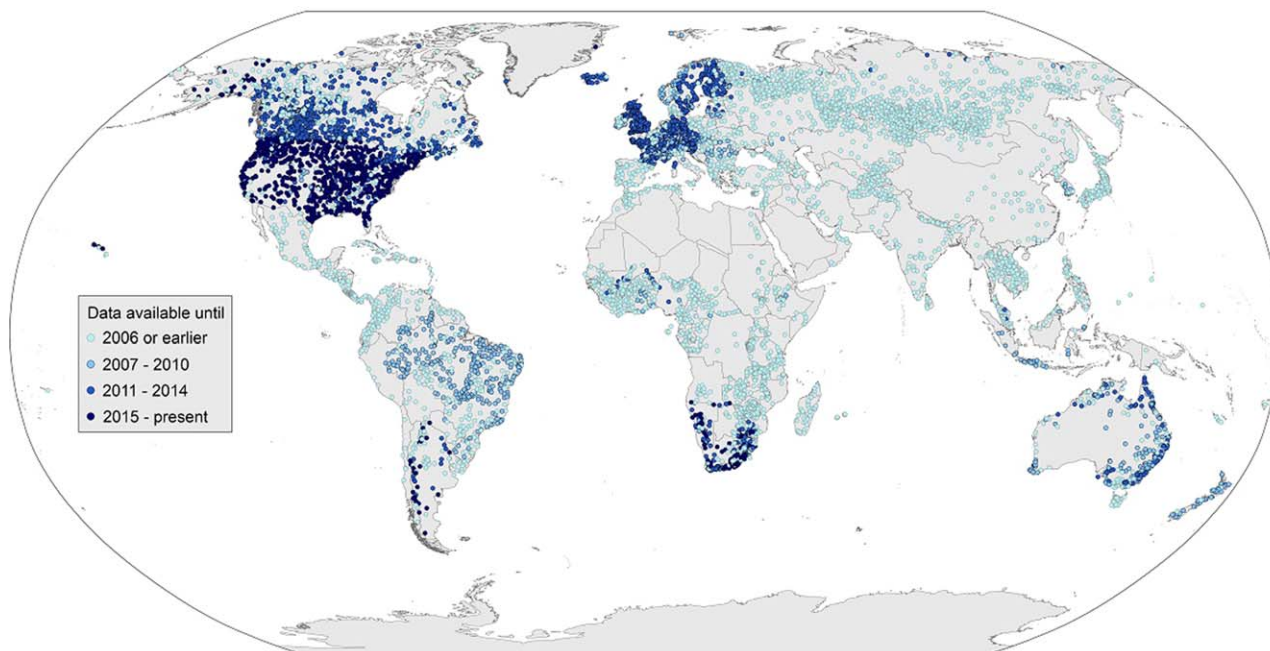
Figure 1. Map of historical gauge data. This map illustrates the rivers with at least some historical data of the kind needed to implement the methods here. The map shows every gauge in the GRDC database as of December 2016, made by querying their gauge catalog. The gauges displayed here have varying degrees of temporal coverage: some (like those provided by the USGS) have decades of history that continue to the present. Others, like those in Russia and in the Nile, have only a limited record. This map also highlights issues of data latency, as very few gauges are provided to the GRDC in near real time.

Scientists have recently turned to satellites to search for this needed flow data. The GRACE satellites have proved hugely effective at tracking water storage change at large scales where changes in water storage like groundwater movement manifest in earth's gravity field (e.g., Lee et al., 2011; Syed et al., 2009), but GRACE cannot provide river discharge at the small watershed scale. The most prevalent technique for using satellites to estimate discharge is to couple satellite observations directly with field measurements. A common algorithm for doing so involves building an empirical relationship between field measurements of discharge and satellite observations of stage, width, or some other fluvial observable (e.g., Ashmore & Sauks, 2006; Bjerklie et al., 2003, 2005; Bjerklie, 2007; Brakenridge et al., 2007; Gilvear et al., 2004; Nathanson et al., 2012; Pan et al., 2016; Pavelsky, 2014; Sichangi et al., 2016; Smith & Pavelsky, 2008; Smith et al., 1996; Tarpanelli et al., 2013; Tourian et al., 2013). In addition to these field calibrated approaches, the forthcoming NASA/CNES Surface Water and Ocean Topography (SWOT) satellite scheduled for launch in 2021 holds promise for estimating discharge without in situ information as demonstrated by using hydraulic model output as a proxy for future simultaneous SWOT observations of water surface elevation and width using a McFLI (Mass conserved Flow Law Inversion) paradigm (Biancamaria et al., 2015; Bonnema et al., 2016; Durand et al., 2008, 2010, 2014, 2016; Garambois & Monnier, 2015; Yoon et al., 2013; Gleason et al., 2017). Should SWOT successfully launch and the discharge inversion techniques developed for it succeed, it would likely usher in a sea-change in hydrologic studies as it could provide (temporally discontinuous) discharge estimates for model calibration and tuning worldwide.

These previous approaches are successful at estimating discharge from remotely sensed observations, yet are unable to reliably estimate flows in ungauged basins either because of the mismatch in scale (GRACE), the need for field calibration of an empirical relationship, or because SWOT does not yet exist. A fourth method of estimating discharge directly from remotely sensed observations is the at-many-stations hydraulic geometry (AMHG) McFLI method described by Gleason and Smith (2014) and Gleason et al. (2014). AMHG is a newly discovered geomorphic phenomenon that links river cross sections in space and time, essentially extending the traditional at-a-station hydraulic geometry that forms the basis for gauging stations in space. AMHG is frequently but not universally observed on natural rivers, and thorough discussion of AMHG as a geomorphic concept is given in the supporting information. Gleason and Smith (2014) first

demonstrated that knowledge of AMHG (derived from remote sensing via a proxy), coupled with multitemporal Landsat imagery and heuristic optimization, could yield discharge estimates with less than 30% error from remote sensing alone. Gleason et al. (2014) further refined this method and revealed that performance of the method was satisfactory for most river morphologies (reporting 26–41% error), but also showed the method to be unsuitable for certain river types (width-invariant and flashy rivers in particular). Gleason et al. (2014) also noted that the proxy for the AMHG relationship seemed weak, which was confirmed by Gleason and Wang (2015) who concluded it to be spurious in their geomorphological analysis of AMHG. Gleason and Wang (2015) showed that AMHG arises from convergence of rating curves, i.e., each individual cross section's AHG power law passes through the same value of width and discharge, and that these congruent values of width and discharge define the AMHG relationship (further confirmed by Shen et al., 2016). Please see the supporting information for further discussion of this concept. As such, some estimate of this rating curve convergence point is now needed to estimate discharge via AMHG. Gleason and Wang (2015) showed that the width convergence point can be approximated via remote sensing, but that the discharge convergence point cannot and needs to be estimated a priori from either precipitation (P) and evapotranspiration (ET) estimates or historical data. Finally, both Bonnema et al. (2016) and Gleason and Hamdan (2015) found that AMHG-based discharge estimation improves substantially when flows are estimated separately for wet and dry seasons in rivers with distinct two-season flow regimes.

The AMHG method can provide discharge estimates in the absence of in situ data, but still falls short of providing the spatially distributed and temporally rich flow information provided by well-calibrated hydrologic models. To that end, we here propose a framework for the synergistic use of remote sensing and hydrologic modeling to estimate discharge in one of the world's most iconic ungauged rivers: The Nile. There is tremendous political and ecological interest in the water balance of the Nile but there are very few public data available, as gauge records end in 1984. We have chosen this important river for demonstration because of its data scarcity, geopolitical complexity, uncertain water balance, and general scientific interest. We selected the Lower Nile in particular (well below Aswan) for demonstration as we have access to a well-developed water balance model for this section. We first review the geopolitical context and historical data availability in this basin. We then ask the question: Can we use AMHG to tune a hydrologic model for an ungauged basin? To answer this question, we estimate Lower Nile discharge using Landsat images and an AMHG-based discharge estimation approach. We first characterize AMHG using satellite-derived P and ET estimates, use this characterized AMHG to estimate discharge from remotely sensed images, and finally tune a water balance model of the Nile (PCR-GLOBWB; Wada et al., 2016) for a time period when the Nile is completely ungauged from an international perspective to assess the effectiveness of this hybrid approach. This represents the longest temporal period and the greatest spatial extent for which the AMHG method has been applied, and as such our modeling is purposefully simple. What results are daily modeled estimates of Lower Nile discharge for the period 1978 to the present day that are among the first streamflow estimates made from remote sensing in the basin. We discuss and contextualize these results as they pertain to both the Nile water balance and the utility of this remote sensing-model synergy in other ungauged river basins.

Importantly, Zeitoun and Allan (2008), among others, have warned against the ineffectiveness of aloof, data-driven solutions to water management challenges in the Nile posed by otherwise well-meaning hydrologists. In this spirit, we do not suggest a solution for Nile water allocation nor do we offer any prescriptive prognosis from our tuned, modeled hydrograph. We also do not attempt to make any water management decisions; rather, we wish to demonstrate the applicability of currently available remotely sensed data for extending historical gauge records and tuning models in regions where gauging information is limited or not available like the Nile.

2. Data and Methods

2.1. Historical Context and Gauge Data

The Nile originates in two different upland areas: the Ethiopian highlands and the Lake Victoria region, which give rise to the Blue and White Nile, respectively. Seventy two percentage of flow in the Nile below the confluence of the two upper Nile Rivers comes from the Blue Nile and the Atbara River (which both arise in Ethiopia), and the Ethiopian highlands alone contribute 86% of the flow in the Nile that reaches Egypt

(Salman, 2011). However, climate change is poised to alter the water balance of the Nile, as precipitation in Ethiopia is driven mainly by the inter-tropical convergence zone that is strongly tied to global energy circulation and seasonal monsoons (Conway, 2000; Swain, 2002; Yohannes, 2009). This physical geography is set against Africa's territorial legacy of postcolonial successor states. Conway et al. (2009) estimate that 90% of the continent's water resources are transboundary, and the Nile is no exception, as there are 11 riparian states within the Nile basin (Figure 2). The White Nile basin contains Burundi, Kenya, Rwanda, Sudan, South Sudan, Tanzania, Uganda, and The Democratic Republic of the Congo en route to its confluence with the Blue Nile at Khartoum. The Blue Nile basin includes Egypt, Ethiopia, Sudan, and South Sudan. These latter four states occupy 85% of the greater Nile basin.

The Nile basin's political and physical geography has led to much contestation for its usage given the number of states included in the basin and the basin's particular imbalance of upland and downstream water resources. Egypt depends almost totally on Nile, and has little alternative to acquire water resources: it thus leverages its postcolonial hegemony to enforce 1959 Nile Waters Agreement to insist on access to well over half of the Nile's annual flow (Dinar, 2012; Luzi, 2010). This has led to a long history of toxic water politics in the region, and thus unsurprisingly, states within the Nile basin do not share flow rate data. There are no publically available gauge data for the Ethiopian highlands, public gauge records on the Atbara River (the major tributary of the Blue Nile) end in 1982, and there are no flow rate data available beyond 2002 at the El Deim station at the border of Ethiopia and Sudan (Conway et al., 2009). Egypt resorts to water balance modeling to assess available water resources and plan for water allocations, but even very simple water balance models are difficult to build without flow rate data (Conway, 1997; Conway et al., 1996), a data deficiency that cannot be overcome by climate data alone (Conway & Hulme, 1993). Despite these difficulties, it is likely that there are gauges within Ethiopia that are currently operational and would provide the data needed to understand how precipitation in the Ethiopian highlands is routed into the Blue Nile and Atbara rivers and eventually to Egypt.
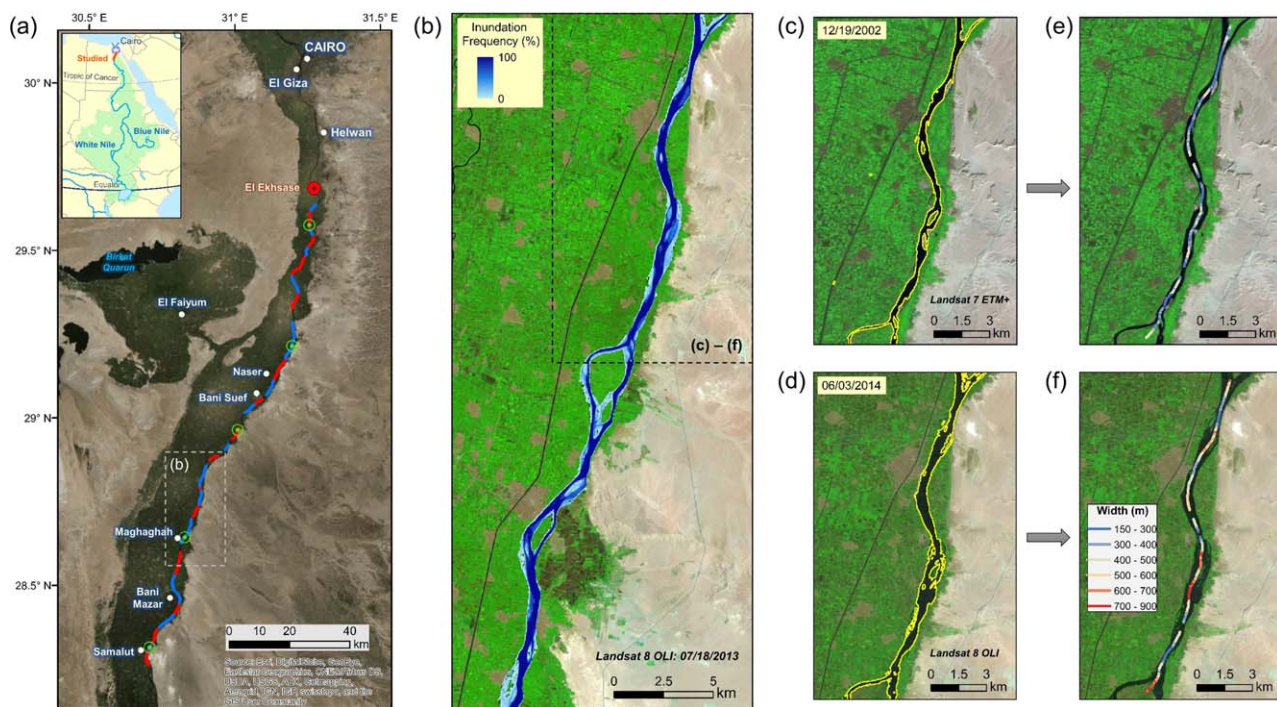

Figure 2. Study reach and width measurements. True and false color composites show our study area and remote sensing process. (a) Studied Lower Nile River (∼180 km) from El Ekhsase station (29.70°N, 31.28°E, red circle) upstream to Samalut (28.28°N, 30.74°E). Widths were calculated in 28 mass-conserved reaches (1–14 km in length) shown as red and blue segments. The five width validation points are marked in green. (b) Mapped inundation frequency along a selected segment during 18 July 2013. (c and d) Examples of inundation extent. (e and f) Widths along reach centerlines using mapped inundation extent in Figures 2c and 2d, respectively (legend in Figure 2f applied to Figure 2e).

The historical gauge data used in this study were obtained from the Global Runoff Data Centre (GRDC; http://www.bafg.de/GRDC/EN/Home/homepage_node.html). Gauged discharge data are available at the El Ekhsase station from 1973 to 1984 (GRDC station ID: 1362100, 29.70°N and 31.28°E, Figure 2a). Later information has not been reported to the GRDC, and no other publically available flow data exist to the best of our knowledge. We opted to use the furthest downstream station possible in order to represent the largest upstream catchment area above the station ($\sim$3.0 million km^2) and its associated maximum impact on transboundary water resources.

2.2. Remotely Sensed Data

Multitemporal remote sensing images were acquired to provide repeated width observations along our study reach, which extends upstream from El Ekhsase to Samalut (Figure 2a). This reach has a total distance of $\sim$180 km and does not have any major tributary confluences. This large reach was further partitioned into 28 finer mass-conserved reaches ($\sim$1–14 km, Figure 2a) chosen to avoid junctions with irrigation conduits or other artificial infrastructure visually identified from high-resolution Google Earth images.

We selected a total of 91 high-quality, cloud-free images acquired from multiple Landsat sensors, including 46 images from the Thematic Mapper (TM), 18 from the Enhanced Thematic Mapper Plus (ETM+), and 27 from the Operational Land Imager (OLI). All images were located on a single tile of Path 176 and Row 40 (in the Worldwide Reference System 2). The temporal coverage of these images spans 1984–2015. The 30 m spatial resolution of Landsat images was generally sufficient to capture width variations along the Lower Nile (Pekel et al., 2016), with a reach-average intra-annual width change of $\sim$320 m or $\sim$10 pixels (see accuracy assessment in section 3.2). The original Landsat Multispectral Scanner (MSS) sensor, which would extend our image record further into the past, was not used due to its coarser spatial resolution.

2.3. Methods
2.3.1. Water Surface Delineation and River Width Measurement

We implemented a highly automated scheme to measure river top widths along the study reaches. We first extracted inundation extent from each Landsat image and then calculated top widths orthogonal to this centerline within each reach (Figures 2b–2f). Accurate inundation extent was extracted using an adaptive water mapping algorithm that simulates how a human operator optimizes the delineation of waterbodies under varying surface conditions. Interested readers are referred to Li and Sheng (2012), Wang et al. (2014), and Sheng et al. (2016) for more detailed descriptions of this algorithm. In brief, the Normalized Difference Water Index (NDWI) (McFeeters, 1996) was first calculated for each Landsat image in order to enhance the presence of surface water (values toward +1) while suppressing the presence of soil/vegetation (values toward −1):

$$NDWI = \frac{G - NIR}{G + NIR} \tag{1}$$

where *G* represents the surface reflectance in the green spectrum (520–600 nm for TM/ETM+ and 530–590 nm for OLI), and *NIR* the reflectance in the near-infrared spectrum (770–900 nm for TM/ETM+ and 850–880 nm for OLI). Candidate water extents were next flagged by segmenting the entire NDWI image using an initial threshold of −0.15. This segmentation was aimed to detect potential waterbodies rather than precisely delineate them. The threshold was purposely assigned to be slightly less than zero to include surface water with high turbidity or aquatic vegetation (thus reducing the initial omission error). Each flagged waterbody was then revisited, and its extent was fine-tuned by an updated segmenting threshold, estimated automatically from the NDWI histogram using pixels in the waterbody vicinity (i.e., a buffer zone). The updated NDWI threshold is, in theory, more adaptive to the local water spectral conditions rather than our initial global discriminant of −0.15. This local-level segmentation was implemented iteratively until the resultant water extent converged, implying that the optimal delineation for this waterbody had been achieved. This algorithm has been shown to be highly robust to common disturbing factors such as turbidity, ice, and aquatic vegetation in different geographic settings (Lyons et al., 2013; Song et al., 2016; Wang et al., 2014). A rigorous quality assurance was further performed on our automated water extents with assistance of a user-interactive mapping tool (Wang et al., 2014) in order to eliminate any remaining mapping errors.

Our extracted water extents (exemplified in Figures 2c and 2d) were next input to RivWidth (v0.4; Pavelsky & Smith, 2008), a commonly applied software tool to automate the calculation of river effective widths (Allen & Pavelsky, 2015; Allen et al., 2013; Miller et al., 2014). In general, RivWidth first applies computational geometry to generate a centerline for any linear water mask. An orthogonal line is next derived at each centerline pixel representing the location of a unique cross section. The total width along each orthogonal is then computed as the effective width at this cross section over a reach length of 30 m (a Landsat image pixel) (Figures 2e and 2f), which was tested to be comparable in quality to manual measurement (Pavelsky & Smith, 2008) (also see section 3.2). We used a static river centerline for all acquired Landsat images (as shown in Figures 2a, 2e, and 2f), in order to ensure that all calculated river widths repeat precisely at well-controlled cross sections.

2.3.2. Discharge Estimation via AMHG

River widths measured in section 2.2.1 were used to estimate Nile River discharge following the basic method described by Gleason and Smith (2014) and Gleason et al. (2014). Readers are referred to this paper's companion supporting information for a thorough discussion of both the theory and application of AMHG as it pertains to this work, and we briefly summarize the method here. AMHG discharge estimation is based on classic at a station hydraulic geometry (AHG), equation (2), where w is width, Q is discharge, and a and b are empirically calibrated parameters:

$$w = aQ^b \qquad (2)$$

The first stage in an AMHG discharge estimation is to characterize AMHG itself. Rather than using the *slope* and *intercept* paradigm of Gleason and Smith (2014) to describe AMHG, we use the Q_c and w_c paradigm introduced by Gleason and Wang (2015), which states that when AMHG is observed, then

$$b = -\frac{\log a}{\log Q_c} + \frac{\log w_c}{\log Q_c} \qquad (3)$$

and then by substitution of equation (2) into equation (3), we arrive at the AMHG equation for flow

$$\log Q = \frac{\log w + b \log Q_c - \log w_c}{b} \qquad (4)$$

where $1/\log Q_c = $ *slope* and $\log w_c / \log Q_c = $ *intercept* as described by Gleason and Smith (2014). Note that equations (3) and (4) are special cases of equation (2) when AMHG is observed, yet they hold simultaneously at all stations of a river, not just a single station as in equation (2). AMHG does not always exist: some rivers do not have either a w_c or a Q_c, making this method inappropriate. This is an active area of future research.

Gleason and Wang (2015) proposed that Q_c and w_c are the points of rating curve convergence: AMHG's geomorphological meaning is that all rating curves of a particular reach pass through the same values of w and Q. Gleason and Wang (2015) then posited that these can be given by the spatial modes of time mean quantities of w and Q, which Shen et al. (2016) noted is a sufficient but not a necessary proposition. w_c (425 m) was thus calculated directly from the Landsat-derived widths from all cross sections (rounded to the nearest tenth in log space per Gleason and Wang (2015), but some a priori estimate of Q was needed to characterize Q_c. We derived Q_c from satellite measures of P and ET to test the efficacy of satellite-model synergy. Precipitation estimates were derived from the gauge-corrected satellite precipitation data sets from the Global Precipitation Climatology Centre (GPCC) (http://www.dwd.de/EN/ourservices/gpcc/gpcc.html). Given the large uncertainty in satellite-based ET estimates, ET was derived from an ensemble of MODIS products for the Nile (Cleugh et al., 2007; Mu et al., 2011, 2013). Thus, Q_c was taken as the long-term mean of this P-ET satellite water balance (3,600 m³/s), and to estimate discharge, equation (4) is used as an objective function in a genetic algorithm (GA) that seeks to solve for Q_c and Q given observed widths. The Nile exhibits a distinct seasonal river flow, but observed flow only varies from ~1,000 to 2,000 m³/s at the monthly time scale. We do not follow a monsoonal separation of wet and dry seasons per previous work on the Ganges River (Bonnema et al., 2016), as the Ganges has a much more pronounced seasonal flow variation. We thus estimate flow across all images and all reaches using the GA. The supporting information details this process for the interested reader (Deb et al., 2002; Ferguson, 1986; Leopold & Maddock, 1953; Phillips, 1990).

2.3.3. Modeling the Nile via PCR-GLOBWB

In order to model spatially and temporally explicit discharge in the Nile, the state-of-the-art hydrological model PCR-GLOBWB was used at a 0.1° by 0.1° spatial resolution (~10 km by ~10 km at the equator)
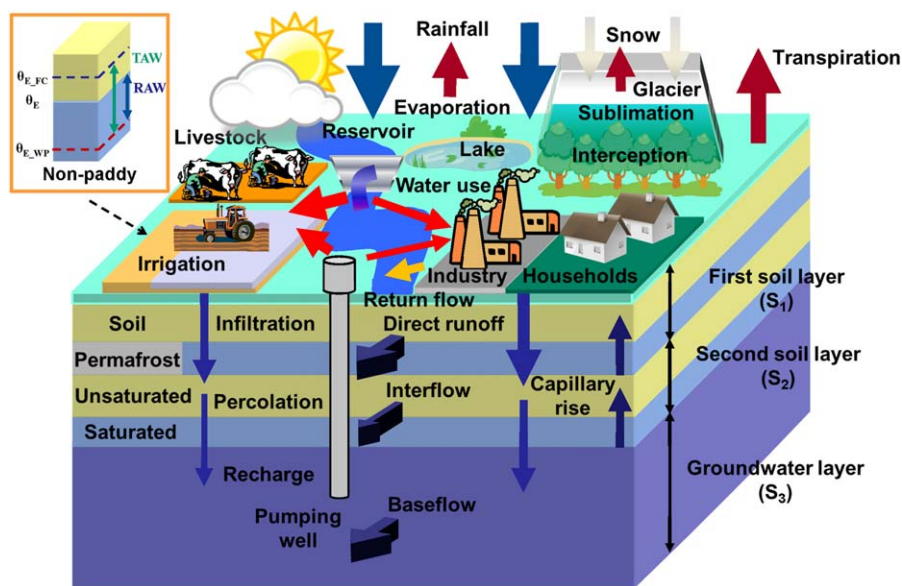
Figure 3. Schematic diagram of the hydrological modeling framework of the PCR-GLOBWB model (Reprinted with permission from Wada et al., 2016). This box diagram represents the vertical structure for the soil hydrology representing the canopy, soil column (stores 1 and 2), and the groundwater reservoir (store 3). Snowmelt is temperature controlled, and potential evapotranspiration is broken down into canopy evaporation, bare soil evaporation, and transpiration that are reduced on the basis of the moisture content of the soil. Drainage from the soil column to the river network occurs via direct runoff, interflow, or subsurface storm flow and base flow. Drainage accumulates as discharge along the drainage network and is subject to a direct gain or loss depending on the precipitation and potential evaporation acting on the freshwater surface. Human water management includes water use from surface water and groundwater, and reservoir regulation is integrated with hydrology at a daily time step.

covering the entire Nile River drainage basin (5°S–35°N and 22°E–41°E) and at a daily temporal resolution (Wada et al., 2014, 2016). This is among the finest spatial resolutions used over the Lower Nile as compared to previous large-scale water balance assessments, and enables us to more precisely depict regional variability in water balance and river discharge. The model runs at a daily temporal resolution with input data that have been parameterized at a 0.1° grid, and input parameters at this enhanced spatial resolution include topography, vegetation, soil properties, and lithology (Wada et al., 2016). Channel characteristics for river routing have also been derived from a high-resolution drainage direction map (HydroSHEDS, http://hydrosheds.cr.usgs.gov/index/php/). Moreover, human water management such as human water use from agriculture (i.e., livestock and irrigation), industry, households, and reservoir regulation have been also parameterized at a 0.1° grid, using the latest available spatially explicit data of livestock densities, irrigated areas, population numbers, and the location of reservoirs (Lehner et al., 2011; Wada et al., 2016). For the extensive description of the basic hydrologic model structure, global forcing data, and associated water use calculation, we refer to Wada et al. (2014, 2016). We briefly present some of the main features of the model and its parameterization at 0.1° in Figure 3 and in supporting information section 3.

2.3.4. Tuning PCR-GLOBWB With AMHG

There are no gauge data available for model calibration for the period 1984 to present, hence the need for this present work. Thus, in order to improve the accuracy of river discharge simulation over the drainage network, we tune the model with AMHG-derived river discharge collected over 1984 to present instead (see section 2.2.2, Table 1). The model time domain is from 1978 to present, so we are therefore tuning the model with discrete discharge estimates made across the latter end of its time domain. We validate the model for a 6 year period of overlap with the gauge where remotely sensed data are not available (1978–1984). Table 1 shows the temporal resolution of key facets of this study, and we remind the reader that there is no temporal overlap between the gauge and the AMHG-derived flows, nor has the gauge been used to estimate discharge or inform AMHG: the gauge remains truly a validation data set. To tune the model, a time-integrated multiplicative correction/tuning factor is calculated for the basin from AMHG river discharge estimates. The multiplicative correction factor is simply calculated as the quotient of the time

Table 1
Time Domains

Data	Resolution	Domain
Landsat images	87 instantaneous images	1984 to present
Gauge	Monthly	1972–1984
Model	Daily	1978 to present

mean of AMHG-derived discharge estimates and the time mean of uncalibrated PCR-GLOBWB discharge simulations for periods where AMHG flows are available: i.e., the mean of the remotely sensed discharge on each day an image was acquired in the period 1984–2015. The long-term average approach has been chosen due to the limited years of AMHG-derived estimates. This multiplicative correction factor is applied to all P and ET values, but is proportionally weighted and applied based on the ratio of P and ET to the total P + ET on the basis of the daily model simulation in order to force runoff over the basin to correct itself toward the AMHG estimates. The tuned runoff (R) is then routed along the river network as described in the previous section. Thus, this tuning scheme assumes that any error in modeled runoff is attributed to P and ET given the water balance equation, assuming no major trend in water storage over the simulation period. This method has been chosen because it is computationally inexpensive, and because we have attributed the errors in the original simulated river discharge to climate forcing rather than model parameters (e.g., calibration) given to the large uncertainty of the uncalibrated modeled hydrograph. Finally, major dams like Aswan affect the seasonality of flow, but do not have large impacts on the mean annual flow of a river by conservation of mass. Thus, without detailed operation rules that are not available for Aswan (or many other dams), our method is likely to produce results that improve flow magnitude but not timing.

3. Results

Figure 4 shows that we were able to successfully tune a hydrologic model of the Nile from remotely sensed data without invoking in situ data. Here, temporally sparse and spatially variable AMHG flow estimations made at 87 discrete times in 28 subreaches of our study area were fed into a global hydrologic model (four out of the original 91 images were removed during preprocessing for having low-width outliers of 0 or
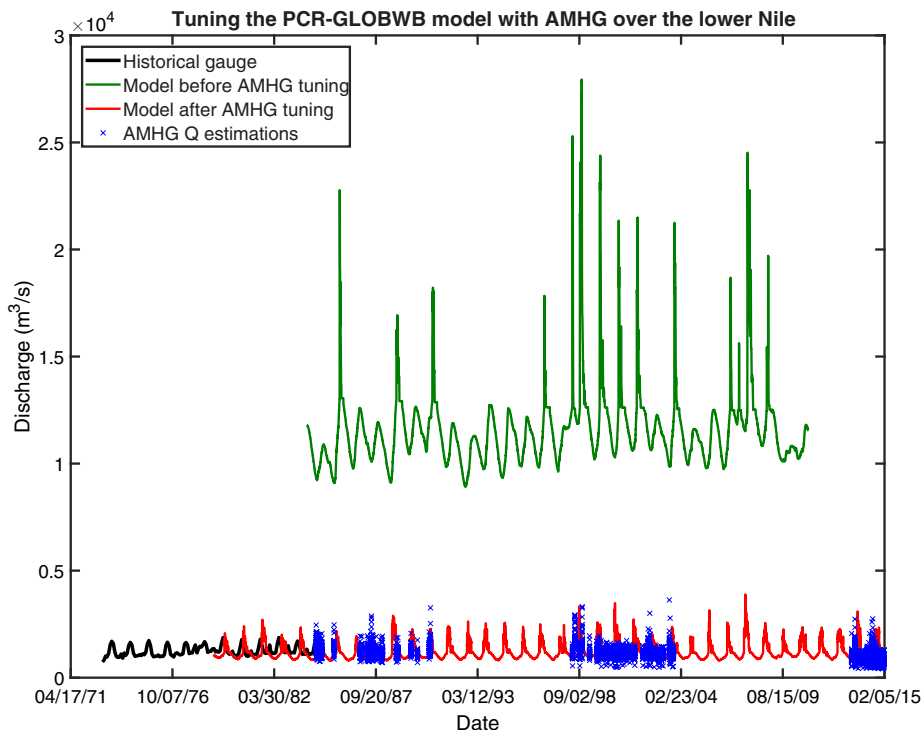

Figure 4. Tuning PCR-GLOBWB with AMHG. This figure shows the substantial improvement gained when using remotely sensed discharge estimates (blue cross) to tune a water balance model of the Nile. The uncalibrated model results (green), which have previously been shown to be accurate for most world basins, are an order of magnitude greater than historical flows (black). After model turning from remote sensing, the new (red) hydrograph shows substantial improvement and agreement with historical gauge flows.

30 m as a result of mapping and width calculation uncertainties, supporting information section 1). The model was adjusted to match the scale of runoff in our remotely sensed flows, and the resultant hydrograph shows an order of magnitude improvement brought about via remotely sensed data alone. The hydrograph is modeled daily, which overcomes limitations of the sparse AMHG flows, and exhibits a 1–2 month flow lag and a negative base flow bias. The RSME of the modeled hydrograph, as validated monthly against the only gauge data available from 1978 to 1984 is 439 m^3/s, and is 270 m^3/s when adding a 2 month lag. Below, we give detailed results as they pertain to the remote sensing and modeling portions of this study.

3.1. AMHG Flow Estimation

Our results indicate that we have made hydrologically useful estimates of flow from remotely sensed data without relying on any in situ data. Remotely sensed flow retrievals ranged in magnitude from 405 to 3,603 m^3/s, matching the scale of historical observations despite being given an initial estimate of Q_c of 3,600 m^3/s. This is a major improvement over previous work, which indicated that the initial choice of Q_c plays a large role in determining estimated discharges and that some in situ data are needed to estimate Q_c (Gleason & Wang, 2015; Gleason et al., 2014). The updated methodology documented in the supporting information was responsible for this improvement, as employing a version of the AMHG method as previously conceived did not return correct-magnitude flows (yielding instead flows centered on the P -ET Q_c of 3,600 m^3/s). The major modifications here include a $\pm 70\%$ variation in expected Q_c, flow limits of 100 and 20,000 m^3/s, and targeted solution selection across the GA Pareto Front. These broad ranges for flow indicate that the GA was free to find solutions that do not at all reflect historical flows (which range from $\sim$1,000 to 2,000 m^3/s), yet the GA still found solutions within the correct scale. Thus, while AMHG flows were highly variable from reach-to-reach and we lack data for a formal validation, the AMHG discharge retrieval here was successful for our purposes. Without contemporaneous validation data, we must assume stationarity of gauge flows to assess the accuracy of AMHG retrievals, and thus our assessment relies only on matching the scale and seasonality of a stationary gauge.

While highly successful for this study, especially considering the absence of in situ data, our AMHG discharge estimations did exhibit broad spatial variability along our 180 km study ready. There were 28 estimation reaches in this study, and each one produces a different estimate of flow for every one of the 87 Landsat images. The vertical differences in AMHG retrievals in Figures 4 and 5 indicates the variability of AMHG flow estimation for a given image, which reflects: (1) true downstream changes in discharge, (2) the different ways that AMHG flow is summarized across the Pareto Front (see supporting information), (3) width mapping errors, (4) the problem of equifinality in the GA, and (5) unaccounted for withdrawals of water for irrigation. AMHG discharges vary by a factor of 3–4 across for our 180 km reach for the same day, despite matching the scale of historical observations quite well (Figure 4). The mean standard deviation of AMHG-derived flow is 295 m^3/s (mean coefficient of variation of 0.25) across all reaches: this reflects the expected one-sigma variability for any given AMHG discharge. The mean AMHG flow through the study reach indicates a peak flow 1–2 months prior to the tuned model, matching the gauge in this respect and indicating no flow lag is observed in AMHG estimates of flow (Figure 5). This is expected, as AMHG flows are derived from observations of width within the reach that reflect true conditions on that day. Our results therefore indicate AMHG may be more reliably used as model tuning data to adjust the scale of runoff rather than as discharge retrievals in their own right for the Nile, although we cannot make this assertion firmly given the absence of validation data.

To assess the quality of our calculated river widths, we selected five equally spaced cross sections through the study reach (Figure 2a), and then randomly sampled 10 acquisition dates for each cross section, forming a total sample of 50 width estimations. By comparing these 50 widths against manual measurements meticulously performed on the source Landsat images, we infer that our automated widths have a mean bias of -28.3 (± 52.0) meters (or $\sim$1–3 pixels) and a $\sim$10% disagreement with manual measurements in width variation ($r^2 = 0.89$). The minor underestimation in width is consistent with the iterative nature of our applied water mapping algorithm which tends to identify only pixels with large water fractions (Lyons et al., 2013; Wang et al., 2014), and the errors in width variation reflect the intrinsic constraint of Landsat's spatial resolution and uncertainties in manual measurements. Given these well-informed error scales, we assert that our calculated Nile widths are sufficient for estimating discharges via AMHG.
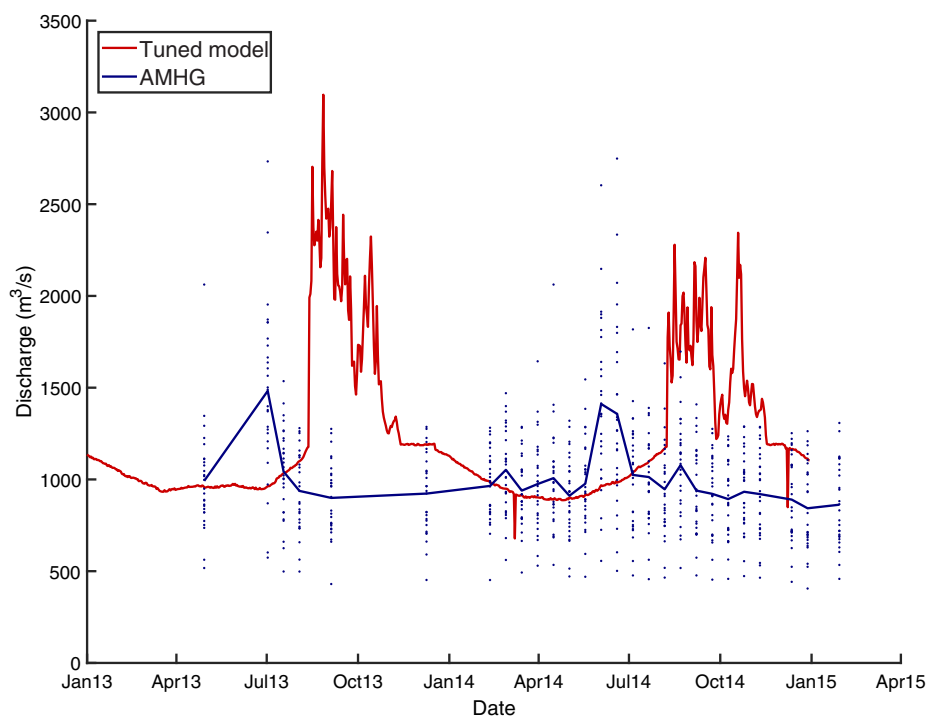
Figure 5. AMHG variability. Each of the 28 blue dots represents an AMHG discharge estimate for a separate reach on a given day with a Landsat image for this subset of the temporal record. The reach-to-reach variability of AMHG is evident, yet the blue lines connecting mean flow through the entire reach indicates that AMHG has a peak flow 2 months before the model, which would suggest they do not have a lag in flow.

3.2. Hybrid AMHG-PCR GLOBWB Results

Tuning the PCR-GLOBWB model with AMHG-derived flows decreased modeled flows by an order of magnitude from uncalibrated model results to more closely align with the historical gauge. Figure 4 shows the tuned hydrograph as compared to an uncalibrated model run over the entire study period, where the benefits of AMHG tuning are self-evident. Figure 6 shows a detailed comparison of the tuned monthly hydrograph against the historical gauge record for the period 1978–1984, before 30 m resolution Landsat images were available. These results show that tuned flows have a 1–2 month lag in peak flow estimation, a monthly Q RMSE of 439 m^3/s (Relative RRMSE 40.8%, computed via summary of a relative residual at each time step), and mean and standard deviation of flow residuals of -145 and 417 m^3/s, respectively. Applying a 2 month lag yields improved monthly RMSE and RRMSE of 270 m^3/s and 25.7%, respectively. Thus, we can attribute roughly half of the error in the hydrograph to errors in seasonality/routing, and half to magnitude errors in flow. This lag is perhaps exacerbated given our lack of knowledge of operation of the Aswan High Dam and other water management decisions (e.g., irrigation), and the lag persists in both the uncalibrated and tuned flows, as expected. Figure 6 also indicates a base flow bias while retaining the ability to match the magnitude of peak flows, and the scale of modeled flows matches the gauge nicely, as guaranteed by our tuning procedure and the scale of AMHG retrievals. This is the only validation period available for this study, as after 1984 the Nile can be considered as ungauged.

These AMHG-tuned results are in stark contrast to the uncalibrated model hydrograph, which has an average mean annual flow (across the entire modeled time domain 1978 to present) of 1.15×10^4 m^3/s compared to the historical gauge average mean annual flow (available 1972–1984) of 1.23×10^3 m^3/s. The uncalibrated hydrograph was created following the procedure described in Wada et al. (2016), save we here used the same P and ET data to force the model as we used to characterize AMHG, and readers are referred to this previous work for detailed description of the modeling procedure. In general, uncalibrated PCR-GLOBWB hydrographs have been shown to be comparable to observed discharge for most world basins, where R^2 (the coefficient-of-determination) is generally over 0.9, and NSC (Nash-Sutcliffe model efficiency coefficient) is over 0.6 (Wada et al., 2016). However, for the Nile, our uncalibrated PCR-GLOBWB R^2 is <0.8
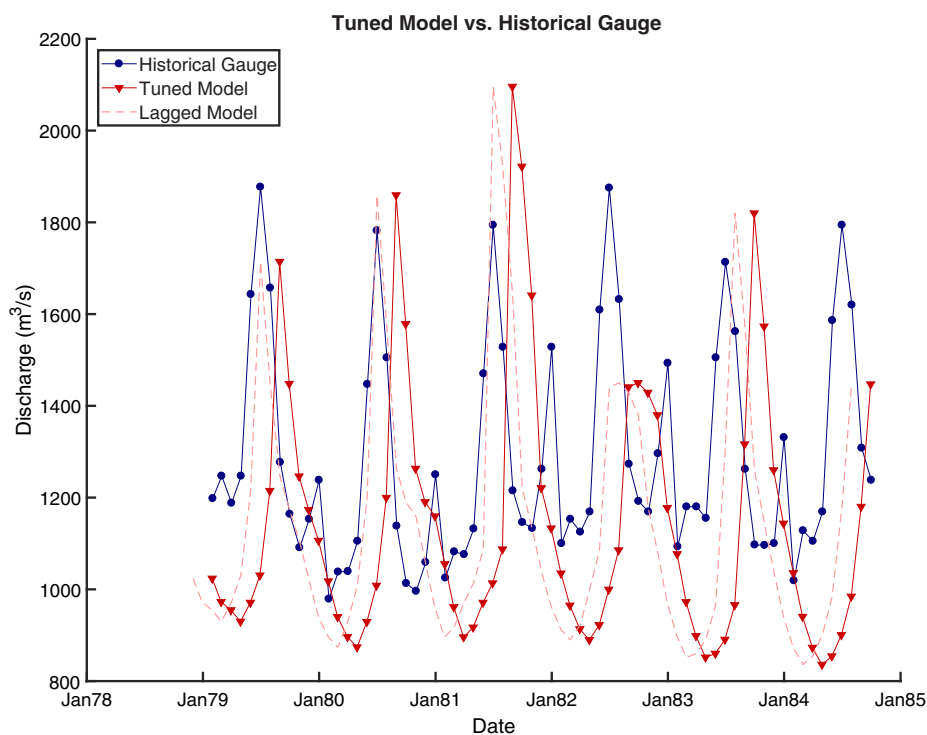
Figure 6. Validation of tuned hydrograph. The monthly comparison shown here indicates that the modeled hydrograph has a 1–2 month seasonal time lag for peak flows and has an RMSE of 449 m^3/s and mean and standard deviation of residuals of -145 and 417 m^3/s, respectively. Lagging the model by 2 months reduces the RMSE to 270 m^3/s. This contrasts sharply with uncalibrated model results that were an order of magnitude larger than gauge flows.

and NSC is <0 for the mean, maximum, and minimum discharges, and simulated mean discharge is an order of magnitude greater than observed mean discharge. Uncalibrated minimum and maximum flows in the Nile overestimate the discharge to a lesser extent, but the deviations from the observations are still substantial (i.e., larger by a factor of 3–4). Including human water management, e.g., accounting for best-estimate accounts of the nonpublicly available irrigation, industrial, and reservoir withdrawals, has been shown to improve overall model performance, but this improvement is limited to about 10% in terms of discharge simulation over the Nile (Wada et al., 2016). Similarly, this same previous work has shown using the gauge-based GPCC P and an ensemble ET product over the Nile (as we have done here) does not substantially improve the overall model performance and discharge simulation, and our results confirm this (Wada et al., 2016). Ultimately, our AMHG-model tuning approach attributes the errors in simulating the Nile discharge to the prescribed climate forcing (i.e., P and ET) rather than model parameters. Therefore, this approach primarily altered the amount of runoff in the water balance components, where excessive runoff has been reduced based on the information obtained from the AMHG-derived estimate.

4. Discussion

4.1. Modeling the Nile

The results of this study indicate that the synergy between multitemporal remote sensing, hydrologic modeling, and the AMHG discharge estimation method can be used to improve modeling of the Lower Nile. While it is difficult to validate the tuned model outside of the overlapping period with the gauge, Figure 4 clearly indicates that tuning the model with remotely sensed flows provided guidance to the model and resulted in more accurate flow estimations. What is particularly interesting is that the combination of the model and AMHG produces results that are more than the sum of their parts: the uncalibrated model had a large bias, while AMHG results are temporally sparse and highly variable reach-to-reach along our study section. Our hybrid approach overcame this AMHG sparseness and variability to guide the model to the correct hydrologic state, where it has a 2 month flow lag and lagged RMSE of 270 m^3/s instead of an

order of magnitude greater RMSE for uncalibrated results and the same lag. This improvement came solely from remotely sensed data products, thus even though the modeled hydrograph is not as accurate as a model calibrated to gauge flows throughout its time domain, our technique holds promise for future water resource applications in ungauged basins.

We have demonstrated substantial improvement in the hydrograph, yet the overall hydrology of the Nile remains poorly understood. Given the lack of available local information of hydrological fluxes including P, ET, runoff, recharge, and irrigation water use, much of our hydrological model simulation is not well constrained. Thus, formal model calibration (as opposed to the tuning here) may not yield hydrologically sound physical parameters (e.g., crop factor, hydraulic conductivity, soil thickness and water storage, and Manning roughness coefficient). In addition, due to the limited observation periods of river discharge (i.e., 1972–1984), model calibration and validation may not even be feasible over the Nile. In general, hydrological models are quite sensitive to climate inputs and this tendency is more obvious in (semi)arid regions, where hydrological fluxes are dominated by a large seasonality (Wada et al., 2014). For the Nile, hydrological variability caused by seasonal climate is further complicated by human water management including irrigation and dam regulation, both of which are included in the model simulation with "best-guess" parameterizations. Ultimately, our approach is still fundamentally limited by observations (as is all modeling), but we have added one novel observation: satellite measurements of width, which we have converted to discharge. The addition of remotely sensed information has substantially improved model results and met our study objectives, even if we cannot distribute this improvement to particular water balance components in the overall hydrology of the basin.

Our tuning approach is simplistic but still shows promise for improved water balance estimates using only publicly accessible data; however, some obvious errors have been noted. The approach primarily reduces excessive runoff and attributes these errors to climate forcing, and does not essentially adjust any model hydrological parameters. Thus, for example, the model errors in routing still persist, which yielded the 1–2 month lag between the tuned and observed discharge. Indeed, the tuned hydrograph exhibited an error of 439 m^3/s, roughly half of which can be attributed to errors in seasonality that persist from forcing to simulation. This error may be reduced by implementing another temporal tuning parameter in the AMHG-model hybrid approach or applying a sinuosity correction (Wu et al., 2012) but given the limited observation periods (∼3 images per year), this needs further consideration. The error in lag time may well be affected by the reservoir regulation at the Aswan dam, which involves human water management factors that are extremely difficult to capture without published management decisions. Errors in hydrograph seasonality are also likely affected by similar concerns, and these need further consideration as to how to improve the current AMHG-model approach. In other words, we expect our current approach to work well in basins where the uncalibrated model hydrograph matches observed seasonality. PCR-GLOBWB, e.g., has been shown to accurately model seasonality for many other major river basins that are in (semi)arid and (sub)-tropical climates. Furthermore, since our approach is simplistic and easily implemented in the modeling framework, a multimodel ensemble approach can be introduced to reduce the ensuing errors that are associated with the model used in this study. Our approach is easily replicable with other hydrological models, which we feel is a strong advantage. In this study, one of our aims has been to provide a simple yet reasonable approach to integrate satellite estimates with model simulation with potential for global coverage, as tested in the Nile. We believe that our simplistic approach is essential to achieve this objective at the global scale.

4.2. The Role of Historic and Remotely Sensed Data

All of the above analysis assumes that the historic gauge record used in this study accurately represents flows, as we use this gauge record as our validation standard. This could be problematic for several reasons. First, gauge records can often contain considerable error, especially at higher flows. Thus, the peak flows as reported by the gauge may misrepresent actual flow for those months. Second, we have no means of assessing AMHG or model performance for the 30 year period after the gauge record ends, and are left assuming stationarity of discharge to perform a qualitative assessment of flows for this period. This assumption seems reasonable in this case, as the modeled hydrographs (both tuned and uncalibrated) and the gauge record itself show stable mean annual flow over time. Despite these limitations, our paradigm for this study seeks to answer the question: *Can we use AMHG to tune a hydrologic model for an ungauged basin?* We can answer this in the affirmative, albeit with caveats, and propose that the techniques

demonstrated here could potentially be applied for the numerous basins worldwide where only historical data are available to the international community (Figure 1).

Our use of remotely sensed data is unique in this study. We employ satellite P and ET estimates in conjunction with width measurements made from Landsat to estimate discharge without calibration from any gauge data. This is especially significant in light of the most common means of employing remote sensing to estimate river discharge: empirically combining remotely sensed data and in situ estimates of discharge. This traditional use of satellite-derived rating curves has been shown to be as accurate as in situ flow measurement when using high-resolution imagery (Pavelsky, 2014), and it is this approach that should be adopted whenever data are available. However, in cases like the Nile, the historical gauge record does not overlap the satellite era (or at least the modern Landsat era), and this technique cannot be used. In contrast, the AMHG approach does not require contemporaneous data, but it has an expected error of at least 26% and has been shown to be susceptible to much larger discharge estimation errors in some cases (Durand et al., 2016; Gleason et al., 2014). These large errors arise from equifinality in an exponential system (equation (2)). Small changes in estimated b values can manifest as order of magnitude changes in flow, and as such the method "jumps" into different mass-conserved solution spaces and has difficulty returning from them. We have overcome this limitation to some degree via methodological improvements as noted in the supporting information, yet the underconstrained nature of the problem leads to large uncertainties in AMHG estimation, especially as Q_c increases. These uncertainties are evident in the spread of discharges estimated from AMHG, which are all of the same scale but vary widely reach to reach. It is impossible to ascertain whether or not these are errors or reflect true conditions.

AMHG discharges were necessary for this study, as using the P -ET water balance to tune the model would not have resulted in as accurate of a hydrograph. Our tuning procedure guarantees that the tuned flows have a long-term mean equivalent to the long-term mean of the tuning data. Thus, tuned flows had a MAF of 1,180 m^3/s versus the mean AMHG flow estimate of 1,170 m^3/s, both of which match mean gauge flow of 1,250 m^3/s. By contrast, using the P-ET water balance to tune the model would have resulted in tuned flows larger than gauge flows by an approximate factor of three (mean P-ET is 3,600 m^3/s). Therefore, the AMHG method showed ability to take this P-ET estimate of mean flow and refine it to match the scale of the gauge without invoking any in situ data. This indicates that while the AMHG method produced highly variable discharge estimates reach to reach and while there are only 87 total discharge estimates for a 30 year period, the tuned model hydrograph that results from their use offer substantial improvement over state of the art modeling of the Nile that would not be possible with standard remote sensing techniques.

Our results also highlight the main utility of remotely sensed discharge estimates, which are frequently characterized (erroneously) as an attempt to replace both gauges and hydrologic models. Indeed, the variability and sparseness of AMHG results herein indicate they are likely not useful for management decisions on their own. These remotely sensed results would improve tremendously if calibrated to a contemporaneous gauge, likely to the point where they may have more use in a management setting. Previously, the AMHG method has only been applied to at most 20 images (although Durand et al., 2016) applied the method to over 300 modeled observations of width), and even extending this to 87 images here leaves large gaps in the hydrograph that render hydrologic analysis of the Nile nearly impossible from this technique alone. By using these AMHG flows as an intermediate product in model tuning, we have filled in these temporal gaps and reduced the uncertainty of flow estimation for the study area, which points the way forward for use of remotely sensed flow estimates from AMHG and future SWOT mission flow estimates. Only through remote sensing, gauge, and model synergy can a complete picture of global water resources emerge.

4.3. Potential for Broader Applications

This method might be reasonably applied to any basin, but can only be validated where there are data available. Figure 1 shows the extent of the GRDC's gauge records- each dot on the map shows a gauge with at least some historical data where there is potential to verify the techniques of this paper. With declining gauging infrastructure worldwide, hydrological modeling and discharge simulation can provide only limited accuracy of regional water availability in semiungauged basins like the Nile. Satellite observations open a new path to monitor water extent and height from space, however, it is imperative to have an efficient algorithm to translate the satellite data for hydrological applications. Our remote sensing-model hybrid

approach combined with the AMHG algorithm could reduce the errors that are inherent to each approach substantially with inexpensive computational usage, which may be favorable for local regional water planners with limited computational capacity, particularly in developing countries. Remotely sensed data assimilation into models may provide another approach, but this needs careful consideration as it has a much higher computational cost and may not work well when only limited satellite imagery is available. Our simple but effective way to combine remote sensing and hydrological modeling is a first exploration, and needs further improvement, but it is easily applicable to any ungauged basin where almost no discharge information is available.

5. Conclusions

The results presented herein indicate that remote sensing can substantially improve modeled hydrographs, even in the absence of gauges. The technique demonstrated here relies on a satellite water balance to parameterize AMHG, and then follows an AMHG methodology to estimate discharge for each of 87 Landsat images. This discharge is then used to tune the PCR-GLOBWB model of the Nile for an ungauged time period. Results herein are promising, and modeled flows improved by an order of magnitude. However, results also indicate that further testing and validation are required (although validation is difficult in ungauged basins), and more sophisticated techniques are needed to better understand resultant changes to hydrological components of the water cycle resulting from this tuning, rather than changes in discharge alone. In addition, the problem is complex: frozen rivers, channelized or canyon rivers with little to no width variations, narrow rivers that are beyond the detection limits of Landsat, cloudiness during a rainy season that may preclude good Landsat coverage, and undetected flow regulation will all render this method less effective or even completely ineffective. The resolution and cloudiness improvements expected from SWOT should address some but not all of these issues. Nevertheless, our results are encouraging for the hydrological community, and hold promise to improve discharge simulation worldwide, regardless of the availability of observation records. Discharge simulations that result from future improved version of this method could then be used for more accurately estimating regional water supply. Finally, our results also point the way forward for use of remote sensing of river discharge, which is often wrongly thought of as an attempt to replace gauges and models as a primary means of assessing water resources. In contrast, our results show that only through synergy of these components can the fullest picture of water resources emerge.

References

Allen, G. H., Barnes, J. B., Pavelsky, T. M., & Kirby, E. (2013). Lithologic and tectonic controls on bedrock channel form at the northwest Himalayan front. *Journal of Geophysical Research: Earth Surface*, *118*, 1806–1825. https://doi.org/10.1002/jgrf.20113

Allen, G. H., & Pavelsky, T. M. (2015). Patterns of river width and surface area revealed by the satellite-derived North America River Width data set. *Geophysical Research Letters*, *42*, 395–402. https://doi.org/10.1002/2014GL062764

Ashmore, P., & Sauks, E. (2006). Prediction of discharge from water surface width in a braided river with implications for at-a-station hydraulic geometry. *Water Resources Research*, *42*, W03406. https://doi.org/10.1029/2005WR003993

Biancamaria, S., Lettenmaier, D. P., & Pavelsky, T. M. (2015). The SWOT mission and its capabilities for land hydrology. *Surveys in Geophys*, *37*(2), 307–337. https://doi.org/10.1007/s10712-015-9346-y

Bjerklie, D. M. (2007). Estimating the bankfull velocity and discharge for rivers using remotely sensed river morphology information. *Journal of Hydrology*, *341*(3–4), 144–155. https://doi.org/10.1016/j.jhydrol.2007.04.011

Bjerklie, D. M., Lawrence Dingman, S., Vorosmarty, C. J., Bolster, C. H., & Congalton, R. G. (2003). Evaluating the potential for measuring river discharge from space. *Journal of Hydrology*, *278*(1–4), 17–38. https://doi.org/10.1016/S0022-1694(03)00129-X

Bjerklie, D. M., Moller, D., Smith, L. C., & Dingman, S. L. (2005). Estimating discharge in rivers using remotely sensed hydraulic information. *Journal of Hydrology*, *309*(1–4), 191–209. https://doi.org/10.1016/j.jhydrol.2004.11.022

Bonnema, M. G., Sikder, S., Hossain, F., Durand, M., Gleason, C. J., & Bjerklie, D. M. (2016). Benchmarking wide swath altimetry-based river discharge estimation algorithms for the Ganges river system. *Water Resources Research*, *52*, 2439–2461. https://doi.org/10.1002/2015WR017296

Brakenridge, G. R., Nghiem, S. V., Anderson, E., & Mic, R. (2007). Orbital microwave measurement of river discharge and ice status. *Water Resources Research*, *43*, W04405. https://doi.org/10.1029/2006WR005238

Cleugh, H. A., Leuning, R., Mu, Q., & Running, S. W. (2007). Regional evaporation estimates from flux tower and MODIS satellite data. *Remote Sensing of Environment*, *106*(3), 285–304. https://doi.org/10.1016/j.rse.2006.07.007

Conway, D. (1997). A water balance model of the Upper Blue Nile in Ethiopia. *Hydrological Sciences Journal*, *42*(2), 265–286. https://doi.org/10.1080/02626669709492024

Conway, D. (2000). The Climate and Hydrology of the Upper Blue Nile River. *The Geographical Journal*, *166*(1), 49–62.

Conway, D., & Hulme, M. (1993). Recent fluctuations in precipitation and runoff over the Nile sub-basins and their impact on main Nile discharge. *Climatic Change*, *25*(2), 127–151. https://doi.org/10.1007/BF01661202

Conway, D., Krol, M., Alcamo, J., & Hulme, M. (1996). Future availability of water in Egypt: The interaction of global, regional, and basin scale driving forces in the Nile Basin. *Ambio*, *25*(5), 336–342.

Conway, D., Persechino, A., Ardoin-Bardin, S., Hamandawana, H., Dieulin, C., & Mahé, G. (2009). Rainfall and water resources variability in sub-Saharan Africa during the twentieth century. *Journal of Hydrometeorology*, *10*(1), 41–59. https://doi.org/10.1175/2008JHM1004.1

Deb, K., Pratap, A., Agarwal, S., & Meyarivan, T. (2002). A fast and elitist multiobjective genetic algorithm: NSGA-II. *IEEE Transactions on Evolutionary Computation*, *6*(2), 182–197. https://doi.org/10.1109/4235.996017

Dinar, S. (2012). The geographical dimensions of hydro-politics: International freshwater in the Middle East, North Africa, and Central Asia. *Eurasian Geography and Economics*, *53*(1), 115–142. https://doi.org/10.2747/1539-7216.53.1.115

Durand, M., Andreadis, K. M., Alsdorf, D. E., Lettenmaier, D. P., Moller, D., & Wilson, M. (2008). Estimation of bathymetric depth and slope from data assimilation of swath altimetry into a hydrodynamic model. *Geophysical Research Letters*, *35*, L20401. https://doi.org/10.1029/2008GL034150

Durand, M., Fu, L.-L., Lettenmaier, D. P., Als, D. E., Rodriguez, E., & Esteban-Fernandez, D. (2010). The Surface Water and Ocean Topography mission: Observing terrestrial surface water and oceanic submesoscale eddies. *Proceedings of the IEEE*, *98*(5), 766–779. https://doi.org/10.1109/JPROC.2010.2043031

Durand, M., Gleason, C. J., Garambois, P. A., Bjerklie, D., Smith, L. C., Roux, H., . . . Vilmin, L. (2016). An intercomparison of remote sensing river discharge estimation algorithms from measurements of river height, width, and slope. *Water Resources Research*, *52*, 4527–4549. https://doi.org/10.1002/2015WR018434

Durand, M., Neal, J., Rodríguez, E., Andreadis, K. M., Smith, L. C., & Yoon, Y. (2014). Estimating reach-averaged discharge for the River Severn from measurements of river water surface elevation and slope. *Journal of Hydrology*, *511*, 92–104. https://doi.org/10.1016/j.jhydrol.2013.12.050

Ferguson, R. I. (1986). Hydraulics and hydraulic geometry. *Progress in Physical Geography*, *10*(1), 1–31. https://doi.org/10.1177/030913338601000101

Garambois, P.-A., & Monnier, J. (2015). Inference of effective river properties from remotely sensed observations of water surface. *Advances in Water Resources*, *79*, 103–120. https://doi.org/10.1016/j.advwatres.2015.02.007

Gilvear, D. J., Davids, C., & Tyler, A. N. (2004). The use of remotely sensed data to detect channel hydromorphology: River Tummel, Scotland. *River Research and Applications*, *20*(7), 795–811. https://doi.org/10.1002/rra.792

Gleason, C. J., & Hamdan, A. N. (2015). Crossing the (watershed) divide: Satellite data and the changing politics of international river basins. *The Geographical Journal*, *183*, 2–15. https://doi.org/10.1111/geoj.12155

Gleason, C. J., Garambois, P. A., & Durand, M. T. (2017). Tracking river flows from space. *EOS: Transactions of the American Geophysical Union*, *98*. https://doi.org/10.1029/2017EO078085

Gleason, C. J., & Smith, L. C. (2014). Toward global mapping of river discharge using satellite images and at-many-stations hydraulic geometry. *Proceedings of the National Academy of Sciences of the United States of America*, *111*(13), 4788–4791. https://doi.org/10.1073/pnas.1317606111

Gleason, C. J., Smith, L. C., & Lee, J. (2014). Retrieval of river discharge solely from satellite imagery and at-many-stations hydraulic geometry: Sensitivity to river form and optimization parameters. *Water Resources Research*, *50*, 9604–9619. https://doi.org/10.1002/2014WR016109

Gleason, C. J., & Wang, J. (2015). Theoretical basis for at-many-stations hydraulic geometry. *Geophysical Research Letters*, *42*, 7107–7114. https://doi.org/10.1002/2015GL064935

Hannah, D. M., Demuth, S., van Lanen, H. A. J., Looser, U., Prudhomme, C., Rees, G., . . . Tallaksen, L. M. (2011). Large-scale river flow archives: Importance, current status and future needs. *Hydrological Processes*, *25*(7), 1191–1200. https://doi.org/10.1002/hyp.7794

Lee, H., Beighley, R. E., Alsdorf, D., Jung, H. C., Shum, C. K., Duan, J., . . . Andreadis, K. (2011). Characterization of terrestrial water dynamics in the Congo Basin using GRACE and satellite radar altimetry. *Remote Sensing of Environment*, *115*(12), 3530–3538. https://doi.org/10.1016/j.rse.2011.08.015

Lehner, B., Liermann, C. R., Revenga, C., Vörösmarty, C., Fekete, B., Crouzet, P., . . . Wisser, D. (2011). High-resolution mapping of the world's reservoirs and dams for sustainable river-flow management. *Frontiers in Ecology and the Environment*, *9*(9), 494–502. https://doi.org/10.1890/100125

Leopold, L. B., & Maddock, T. (1953). *The hydraulic geometry of stream channels and some physiographic implications*. Washington, DC: United States Geological Survey.

Li, J., & Sheng, Y. (2012). An automated scheme for glacial lake dynamics mapping using Landsat imagery and digital elevation models: A case study in the Himalayas. *International Journal of Remote Sensing*, *33*(16), 5194–5213. https://doi.org/10.1080/01431161.2012.657370

Luzi, S. (2010). Driving forces and patterns of water policy making in Egypt. *Water Policy*, *12*(1), 92–113. https://doi.org/10.2166/wp.2009.052

Lyons, E. A., Sheng, Y., Smith, L. C., Li, J., Hinkel, K. M., Lenters, J. D., & Wang, J. (2013). Quantifying sources of error in multitemporal multisensor lake mapping. *International Journal of Remote Sensing*, *34*(22), 7887–7905. https://doi.org/10.1080/01431161.2013.827343

McFeeters, S. K. (1996). The use of the Normalized Difference Water Index (NDWI) in the delineation of open water features. *International Journal of Remote Sensing*, *17*(7), 1425–1432. https://doi.org/10.1080/01431169608948714

Miller, F. M., Pavelsky, T. M., & Allen, G. H. (2014). Quantifying river form variations in the Mississippi Basin using remotely sensed imagery. *Hydrology and Earth System Sciences Discussions*, *11*, 3599–3636. https://doi.org/10.5194/hess-18-4883-2014

Mu, Q., Zhao, M., & Running, S. W. (2013). *MODIS global terrestrial evapotranspiration (ET) product (NASA MOD16A2/A3) algorithm theoretical basis document collection 5* (Tech. Rep. 1184). Washington, DC: NASA. Retrieved from https://modis-land.gsfc.nasa.gov/pdf/MOD16-ATBD.pdf

Mu, Q. M., Zhao, M., & Running, S. W. (2011). Improvements to a MODIS global terrestrial evapotranspiration algorithm. *Remote Sensing of Environment*, *115*(8), 1781–1800. https://doi.org/10.1016/j.rse.2011.02.019

Nathanson, M., Kean, J. W., Grabs, T. J., Seibert, J., Laudon, H., & Lyon, S. W. (2012). Modelling rating curves using remotely sensed LiDAR data. *Hydrological Processes*, *26*(9), 1427–1434. https://doi.org/10.1002/hyp.9225

Oki, T., & Kanae, S. (2006). Global hydrological cycles and world water resources. *Science*, *313*(5790), 1068–1072. https://doi.org/10.1126/science.1128845

Pan, F., Wang, C., & Xi, X. (2016). Constructing river stage-discharge rating curves using remotely sensed river cross-sectional inundation areas and river bathymetry. *Journal of Hydrology*, *540*, 670–687. https://doi.org/10.1016/j.jhydrol.2016.06.024

Pavelsky, T. M. (2014). Using width-based rating curves from spatially discontinuous satellite imagery to monitor river discharge. *Hydrological Processes*, *28*(6), 3035–3040. https://doi.org/10.1002/hyp.10157

Pavelsky, T. M., & Smith, L. C. (2008). RivWidth: A software tool for the calculation of river widths from remotely sensed imagery. *IEEE Geoscience and Remote Sensing Letters*, *5*(1), 70–73.

Pekel, J., Cottam, A., Gorelick, N., & Belward, A. S. (2016). High-resolution mapping of global surface water and its long-term changes. *Nature*, *540*, 418–422. https://doi.org/10.1038/nature20584

Phillips, J. D. (1990). The instability of hydraulic geometry. *Water Resources Research*, *26*(4), 739–744. https://doi.org/10.1029/WR026i004p00739

Salman, S. M. A. (2011). The new state of South Sudan and the hydro-politics of the Nile Basin. *Water International*, *36*(2), 154–166. https://doi.org/10.1080/02508060.2011.557997

Shen, C., Wang, S., & Liu, X. (2016). Geomorphological significance of at-many-stations hydraulic geometry. *Geophysical Research Letters*, *43*, 3762–3770. https://doi.org/10.1002/2016GL068364

Sheng, Y., Song, C., Wang, J., Lyons, E. A., Knox, B. R., Cox, J. S., & Gao, F. (2016). Representative lake water extent mapping at continental scales using multi-temporal Landsat-8 imagery. *Remote Sensing of Environment*, *185*, 129–141. https://doi.org/10.1016/j.rse.2015.12.041

Sichangi, A. W., Wang, L., Yang, K., Chen, D., Wang, Z., Li, X., . . . Kuria, D. (2016). Estimating continental river basin discharges using multiple remote sensing data sets. *Remote Sensing of Environment*, *179*, 36–53. https://doi.org/10.1016/j.rse.2016.03.019

Smith, L. C., Isacks, B. L., Bloom, A. L., & Murray, A. B. (1996). Estimation of discharge from three braided rivers using synthetic aperture radar satellite imagery: Potential application to ungaged basins. *Water Resources Research*, *32*(7), 2021–2034. https://doi.org/10.1029/96WR00752

Smith, L. C., & Pavelsky, T. M. (2008). Estimation of river discharge, propagation speed, and hydraulic geometry from space: Lena River, Siberia. *Water Resources Research*, *44*, W03427. https://doi.org/10.1029/2007WR006133

Song, C., Sheng, Y., Ke, L., Nie, Y., & Wang, J. (2016). Glacial lake evolution in the southeastern Tibetan Plateau and the cause of rapid expansion of proglacial lakes linked to glacial-hydrogeomorphic processes. *Journal of Hydrology*, *540*, 504–514. https://doi.org/10.1016/j.jhydrol.2016.06.054

Swain, A. (2002). The Nile River Basin initiative: Too many cooks, too little broth. *SAIS Review*, *22*(2), 293–308. https://doi.org/10.1353/sais.2002.0044

Syed, T. H., Famiglietti, J. S., & Chambers, D. P. (2009). GRACE-based estimates of terrestrial freshwater discharge from basin to continental scales. *Journal of Hydrometeorology*, *10*(1), 22–40. https://doi.org/10.1175/2008jhm993.1

Tarpanelli, A., Brocca, L., Lacava, T., Melone, F., Moramarco, T., Faruolo, M., . . . Tramutoli, V. (2013). Toward the estimation of river discharge variations using MODIS data in ungauged basins. *Remote Sensing of Environment*, *136*, 47–55. https://doi.org/10.1016/j.rse.2013.04.010

Tourian, M. J., Sneeuw, N., & Bardossy, A. (2013). A quantile function approach to discharge estimation from satellite altimetry (ENVISAT). *Water Resources Research*, *49*, 4174–4186. https://doi.org/10.1002/wrcr.20348

Vörösmarty, C. J., McIntyre, P. B., Gessner, M. O., Dudgeon, D., Prusevich, A., Green, P., . . . Davies, P. M. (2010). Global threats to human water security and river biodiversity. *Nature*, *467*(7315), 555–561. https://doi.org/10.1038/nature09440

Wada, Y., de Graaf, I. E. M., & van Beek, L. P. H. (2016). High-resolution modeling of human and climate impacts on global water resources. *Journal of Advances in Modeling Earth Systems*, *8*, 735–763. https://doi.org/10.1002/2015MS000618

Wada, Y., Wisser, D., & Bierkens, M. F. P. (2014). Global modeling of withdrawal, allocation and consumptive use of surface water and groundwater resources. *Earth System Dynamics*, *5*(1), 15–40. https://doi.org/10.5194/esd-5-15-2014

Wang, J., Sheng, Y., & Tong, T. S. D. (2014). Monitoring decadal lake dynamics across the Yangtze Basin downstream of Three Gorges Dam. *Remote Sensing of Environment*, *152*, 251–269. https://doi.org/10.1016/j.rse.2014.06.004

Wu, H., Kimball, J. S., Li, H., Huang, M., Leung, L. R., & Adler, R. F. (2012). A new global river network database for macroscale hydrologic modeling. *Water Resources Research*, *48*, W09701. https://doi.org/10.1029/2012WR012313

Yohannes, O. (2009). Hydro-politics in the Nile basin: In search of theory beyond realism and neo-liberalism. *Journal of Eastern African Studies*, *3*(1), 74–93. https://doi.org/10.1080/17531050802682788

Yoon, Y., Durand, M., Merry, C. J., & Rodríguez, E. (2013). Improving temporal coverage of the SWOT mission using spatiotemporal kriging. *IEEE Journal of Selected Topics in Applied Earth Observations and Remote Sensing*, *6*(3), 1719–1729. https://doi.org/10.1109/JSTARS.2013.2257697

Zeitoun, M., & Allan, T. (2008). Applying hegemony and power theory to transboundary water analysis. *Water Policy*, *10*(S2), 3–12.